

H_0 Tension and the Phantom Regime: A Case Study In Terms of $f(T)$ GravityAMR EL-ZANT,¹ WALEED EL HANAFY,^{1,2} AND SHERIF ELGAMMAL¹¹Centre for theoretical physics, the British University in Egypt, 11837 - P.O. Box 43, Egypt²Egyptian Relativity Group (ERG), Cairo University, Giza 12613, Egypt

ABSTRACT

We propose an $f(T)$ teleparallel gravity theory including a torsional infrared (IR) correction. We show that the governing Friedmann's equations of a spatially flat universe include a phantom-like effective dark energy term sourced by the torsion IR correction. As has been suggested, this phantom phase does indeed act as to reconcile the tension between local and global measurements of the current Hubble value H_0 . The resulting cosmological model predicts an electron scattering optical depth $\tau_e \approx 0.058$ at reionization redshift $z_{re} \sim 8.1$, in agreement with observations. The predictions are however in contradiction with baryon acoustic oscillations (BAO) measurements, particularly the distance indicators. We argue that this is the case with any model with a phantom dark energy model that has effects significant enough at redshifts $z \lesssim 2$ as to be currently observable. The reason being that such a scenario introduces systematic differences in terms of distance estimates in relation to the standard model; e.g., if the angular diameter distance to the recombination era is to be kept constant while H_0 is increased in the context of a phantom scenario, the distances there are systematically overestimated to all objects at redshifts smaller than recombination. But no such discrepancies exist between Λ CDM predictions and current data for $z \lesssim 2$.

Keywords: Cosmology – dark energy – modified gravity – galaxies – CMB – SNIa – BAO – reionization

1. INTRODUCTION

Cosmological observations clearly confirm that our universe has speeded up its expansion as of a few billion years ago [Riess et al. \(1998\)](#); [Perlmutter et al. \(1999\)](#), with transition redshift $0.67 \lesssim z_{tr} \lesssim 0.87$ [Farooq et al. \(2017\)](#). In the context of general relativity (GR), explaining this phenomenon requires the introduction of a cosmological constant or a negative pressure component in the field equations, referred to as the dark energy. Several recent analyses, c.f. [Planck collaboration XIII \(2016\)](#), show that this component represents $\sim 69\%$ of the energy density in the universe. The complementary components consist of $\sim 26\%$ and pressureless dark matter $\sim 5\%$ baryons.

Since the dark energy effects are felt on the cosmic scales, they are naturally tied to the gravitational interaction and its description. In GR this involves the field equations

$$\frac{1}{\kappa^2} \mathfrak{G}_{\mu\nu} = \mathfrak{T}_{\mu\nu}, \quad (1)$$

where $\mathfrak{G}_{\mu\nu}$ is Einstein tensor, $\mathfrak{T}_{\mu\nu}$ is the energy-momentum tensor of the matter components; the coupling constant κ , in the natural units ($c = \hbar = k_B = 1$), can be related to the Newtonian constant G by $\kappa = \sqrt{8\pi G}$. To explain the late cosmic acceleration, one should represent the dark en-

ergy component $\mathfrak{T}_{\mu\nu}^{DE}$ as an additional term in Einstein's field equations as

$$\frac{1}{\kappa_{eff}^2} \mathfrak{G}_{\mu\nu} = \mathfrak{T}_{\mu\nu} + \mathfrak{T}_{\mu\nu}^{DE} \equiv \mathfrak{T}_{\mu\nu}^{eff}, \quad (2)$$

where the effective coupling constant κ_{eff} reduces to the constant κ at the GR limit and $\mathfrak{T}_{\mu\nu}^{eff}$ is the total energy-momentum tensor. The additional term $\mathfrak{T}_{\mu\nu}^{DE}$ in Eq. (2) can be sourced either by matter (physical) or gravitational (geometrical) sectors.

(i) In the former case, the cosmological constant Λ is the simpler scenario for the dark energy. This constant is equivalent to a negative pressure term in Friedmann equations with equation of state parameter fixed to a value $w_\Lambda = -1$, allowing the universe to perform a transition from a decelerated expansion epoch dominated by cold dark matter (CDM) to an accelerated expansion dominated by Λ -dark energy, in agreement with observations. Although this Λ CDM model fits well with a wide range of observations, it lacks adequate theoretical underpinning. Indeed, it entails several puzzling issues; e.g. the cosmic coincidence problem and the enormous discrepancy between its theoretical and observational values. On the other hand, an alternative to the cosmological constant consists of dynamical dark energy, akin to inflaton fields, which can be described as a canonical scalar field ϕ minimally coupled to gravity with fixed or dynamical equation of state parameter $-1 < w_\phi < -1/3$.

(ii) When $\mathfrak{T}_{\mu\nu}^{DE}$ is sourced by the gravitational sector, one needs to modify the GR equations, as in GR all geometrical terms but $\mathfrak{G}_{\mu\nu}$ are collected in the right hand side of the field equations (2). Extensions proposed in order to fulfill this include those built on the basis of Riemannian geometry (curvature based theories), such as Gauss-Bonnet and $f(R)$ theories [De Felice & Tsujikawa \(2010\)](#); [Clifton et al. \(2012\)](#); [Capozziello & De Laurentis \(2011\)](#), while others are constructed in the context of Weitzenböck geometry (torsion based theories); e.g. new general relativity, teleparallel gravity, $f(T)$ theories [Cai et al. \(2016\)](#).

As noted by [Sahni & Starobinsky \(2006\)](#), the field equations (2) put both physical and geometrical dark energies on equal footing. Nevertheless, they represent fundamentally different physical descriptions; exploration of alternative cosmological models based on modified gravity are thus motivated by theoretical considerations as well as empirical anomalies listed in [Di Valentino et al. \(2016a\)](#).

Perhaps the most significant anomaly is embodied in the apparent inconsistency of the locally measured value of the Hubble parameter and that inferred from Cosmic Microwave Background (CMB) observations. It is on this that we focus in this paper, showing how cosmological observations could be made consistent in terms of $f(T)$ theories of gravity with infrared corrections. The latest released data sets suggest that there is in fact no concordance value for the current Hubble value H_0 . The local measurements (SNIa and HST) give $H_0 > 70$ km/s/Mpc [Anderson et al. \(2014\)](#); [Riess et al. \(2016, 2018\)](#); [Riess et al. \(2018\)](#), on the contrary the global (CMB) measurements give $H_0 < 70$ km/s/Mpc [Bennett et al. \(2013\)](#); [Planck collaboration I \(2016\)](#); [Planck collaboration XIII \(2016\)](#). As the accuracy on both tracks has increased, the tension between these, instead of disappearing, has crossed over to 3.8 standard deviations [Riess et al. \(2018\)](#). So far no source of systematic uncertainty has been pinpointed to explain the discrepancy of the measurements of the Hubble constant. This being the case, it seems natural to investigate new physical inputs, which could restore consistency of the two tracks. However, major changes due to new physics are not supported by the CMB power spectrum.

Possible extensions to the Λ CDM scenario that have been suggested in order to resolve the aforementioned tension, include invoking a larger neutrino effective number $N_{eff} \sim 3.5$, i.e. the possibility of a dark radiation component (the standard value is $N_{eff} = 3.04$). A second avenue involves a phantom dark energy component with an equation of state $w_{DE} \lesssim -1.1$. This could bring the Planck constraint into better agreement with higher values of the Hubble constant. By varying both parameters simultaneously, it has been shown that there is no privilege for dark radiation if allowance is made for dynamical dark energy [Di Valentino et al. \(2016b, 2017b\)](#); [Huang & Wang \(2016\)](#); [Zhao et al. \(2017\)](#). Phantom energy can be shown to also ameliorate the age conflict [Cepa \(2004\)](#).

Several analyses have in fact favored such a phantom dark energy scenario (e.g., [Sahni et al. \(2008, 2014\)](#);

[Huang & Wang \(2016\)](#); [Di Valentino et al. \(2016b, 2017a,b\)](#); [Wang et al. \(2017\)](#); [Zhao et al. \(2017\)](#)). However, if one insists to work within the GR framework, and assumes the phantom dark energy to be sourced by the matter sector (e.g. canonical scalar field), ghost instability would not be avoidable due to violation of the dominant energy condition [Carroll et al. \(2003, 2005\)](#); [Ludwick \(2017\)](#). This being the case, the choice of the gravity sector as a source of $\mathfrak{T}_{\mu\nu}^{DE}$ is preferable. The latter choice requires a modified gravity framework. In this paper, within the frame of the $f(T)$ modified gravity, we argue that the torsional IR correction is a good candidate to source the phantom-like dark energy. Subsequently, it could resolve the current tension in measuring the Hubble constant.

In Section 2, we revisit the teleparallel geometry and briefly discuss $f(T)$ gravity. In Section 3, we derive the modified Friedmann's equations of the torsional IR correction obtaining the Hubble-redshift relation. In Section 4, we adopt the dynamical system approach showing that the governing equation is as a one-dimensional autonomous system. This allows to analyze its phase portrait and extract some useful information. We show that the model predicts a transitional redshift compatible with observations. Also, we determine the phantom-like nature of the torsional counterpart. Moreover, we find that the model predicts an age of the universe compatible with observations. In Section 5, we fix the model parameters. We show that the torsional IR model reconciles CMB with the local value of H_0 . In addition, we confront the model with other measured parameters, the electron scattering optical depth τ_e . However, the model is in serious tension with the BAO observations, in particular the angular distance measures. We argue that phantom/phantom-like DE models, in principle, cannot solve the conflict with BAO observations. In Section 6, we conclude the present work. We add Appendix A, for some particular values of the model parameters, to give explicit forms of some useful cosmological parameters, time-redshift relation, density parameters and comoving volume element. Also, we show that the scalar fluctuation propagates with a sound speed $0 \leq c_s \leq 1$ at all time.

2. $f(T)$ TELEPARALLEL GRAVITY

In this section, we give a brief description of teleparallel geometry (for more detail see [Aldrovandi & Pereira \(2013\)](#)) and summarize some of the modifications of the Friedmann equations that can come about in the context $f(T)$ gravity generalization.

In a 4-dimensional C^∞ -manifold (\mathcal{M}, e_a) , where e_a are four linear independent vector (tetrad, vierbein) fields defined on \mathcal{M} , the vierbein fields fulfill the conditions $e_a^\mu e^\alpha_\mu = \delta^\alpha_a$ and $e_a^\mu e^\mu_b = \delta^a_b$, where μ denotes the co-ordinate components.

Two approaches can be taken to construct two different geometries on \mathcal{M} . The first is to define the Riemannian geometry by constructing the metric tensor

$$g_{\mu\nu} \equiv \eta_{ab} e^a_\mu e^b_\nu, \quad (3)$$

where η_{ab} is the Minkowski metric on the tangent space of \mathcal{M} . Consequently, one can define the Levi-Civita symmetric connection $\tilde{\Gamma}^\alpha_{\mu\nu} = \frac{1}{2}g^{\alpha\sigma}(\partial_\nu g_{\mu\sigma} + \partial_\mu g_{\nu\sigma} - \partial_\sigma g_{\mu\nu})$ and in fact the full machinery of the Riemannian geometry.

The second approach is to define the teleparallel geometry by constructing the nonsymmetric (Weitzenböck) linear connection straightforwardly from the vierbein that is $\Gamma^\alpha_{\mu\nu} \equiv e_a^\alpha \partial_\nu e^a_\mu = -e_a^\alpha \partial_\nu e^a_\mu$, where the vierbein are parallel with respect to this connection $\nabla_\nu e_a^\mu \equiv 0$, and the differential operator ∇_ν denotes the covariant derivative associated to the Weitzenböck connection. Since $\Gamma^\alpha_{\mu\nu}$ is non-symmetric, it defines the torsion tensor $T^\alpha_{\mu\nu} \equiv \Gamma^\alpha_{\nu\mu} - \Gamma^\alpha_{\mu\nu} = e_a^\alpha (\partial_\mu e^a_\nu - \partial_\nu e^a_\mu)$. However, its curvature vanishes identically. Also, the contortion tensor is given by $K^\alpha_{\mu\nu} \equiv \Gamma^\alpha_{\mu\nu} - \tilde{\Gamma}^\alpha_{\mu\nu} = e_a^\alpha \tilde{\nabla}_\nu e^a_\mu$, where the differential operator $\tilde{\nabla}_\nu$ denotes the covariant derivative associated to the Levi-Civita connection. In addition, the torsion and the contortion tensors satisfy the following useful relations $T_{\alpha\mu\nu} = K_{\alpha\mu\nu} - K_{\alpha\nu\mu}$, while $K_{\alpha\mu\nu} = \frac{1}{2}(T_{\nu\alpha\mu} + T_{\alpha\mu\nu} - T_{\mu\alpha\nu})$, where $T_{\mu\nu\sigma} = g_{\mu\epsilon} T^\epsilon_{\nu\sigma}$.

In teleparallel geometry, the teleparallel torsion scalar

$$T \equiv T^\alpha_{\mu\nu} S^{\mu\nu}_\alpha, \quad (4)$$

is equivalent to the Ricci scalar R up to a total derivative term. In the above, the superpotential tensor $S_\alpha^{\mu\nu}$ is defined as

$$S_\alpha^{\mu\nu} = \frac{1}{2}(K^{\mu\nu}_\alpha + \delta^\mu_\alpha T^{\beta\nu}_\beta - \delta^\nu_\alpha T^{\beta\mu}_\beta). \quad (5)$$

Use the action

$$S = \int d^4x |e| (\mathcal{L}_g + \mathcal{L}_m), \quad (6)$$

where $|e| = \sqrt{-g} = \det(e_\mu^a)$, also we use \mathcal{L}_g and \mathcal{L}_m to represent the lagrangians of gravity and matter, respectively. Since the teleparallel torsion scalar (4) differs from the Ricci scalar R by a total derivative term, the field equations that transpire when using T (in the Einstein-Hilbert action as the gravitation lagrangian) are just equivalent to those with R . This is the Teleparallel Equivalent of General Relativity (TEGR) theory of gravity.

2.1. The matter sector

By varying \mathcal{L}_m with respect to the tetrad fields (which has been shown that it is equivalent to vary with respect to the metric [de Andrade & Pereira \(1998\)](#)), enables one to define the stress-energy tensor of a perfect fluid as

$$\mathfrak{T}_{\mu\nu} = e_{a\mu} \left(-\frac{1}{e} \frac{\delta \mathcal{L}_m}{\delta e_a^\nu} \right) = \rho u_\mu u_\nu + p(u_\mu u_\nu + g_{\mu\nu}), \quad (7)$$

where u^μ is the 4-velocity unit vector of the fluid.

2.2. The gravity sector

In the Einstein-Hilbert action, the TEGR has been generalized by replacing T by an arbitrary $f(T)$ function

[Bengochea & Ferraro \(2009\)](#); [Linder \(2010\)](#); [Bamba et al. \(2010, 2011\)](#) similar to the $f(R)$ generalization. The $f(T)$ Lagrangian is

$$\mathcal{L}_g = \frac{1}{2\kappa^2} f(T). \quad (8)$$

By varying the action containing the Lagrangian \mathcal{L}_g with respect to the tetrad fields we obtain the tensor

$$\mathfrak{H}_{\mu\nu} = e_{a\mu} \left(\frac{1}{e} \frac{\delta \mathcal{L}_g}{\delta e_a^\nu} \right) = \frac{1}{2\kappa^2} e_{a\mu} \left(\frac{1}{e} \frac{\delta f(T)}{\delta e_a^\nu} \right). \quad (9)$$

This gives rise to [Li et al. \(2011\)](#)

$$\mathfrak{H}_{\mu\nu} = \frac{1}{\kappa^2} \left(f_T \mathfrak{G}_{\mu\nu} + \frac{1}{2} g_{\mu\nu} (f - T f_T) + f_{TT} S_{\nu\mu\rho} \nabla^\rho T \right), \quad (10)$$

where f_T and f_{TT} , stand for $f_T = \frac{df(T)}{dT}$ and $f_{TT} = \frac{d^2 f(T)}{dT^2}$ respectively.

2.3. The field equations

Using Eqs. (7) and (10), the variation of the total action (6) with respect to the tetrad fields gives the $f(T)$ gravity field equations

$$\mathfrak{H}_\mu{}^\nu = \mathfrak{T}_\mu{}^\nu. \quad (11)$$

Equivalently, by substituting from Eq. (10), it can be written as

$$\frac{1}{\kappa_{eff}^2} \mathfrak{G}_{\mu\nu} = \mathfrak{T}_{\mu\nu} + \mathfrak{T}_{\mu\nu}^{DE}, \quad (12)$$

where

$$\begin{aligned} \kappa_{eff}^2 &= \frac{\kappa^2}{f_T}, \\ \mathfrak{T}_{\mu\nu}^{DE} &= \frac{1}{\kappa^2} \left(\frac{1}{2} g_{\mu\nu} (T f_T - f) - f_{TT} S_{\nu\mu\rho} \nabla^\rho T \right). \end{aligned} \quad (13)$$

It is clear that the general relativistic limit is recovered by setting $f(T) = T$, where $\kappa_{eff} \rightarrow \kappa$ and $\mathfrak{T}_{\mu\nu}^{DE}$ vanishes. This allows one to deal with the torsional dark energy on equal footing with the physical one. Although the teleparallel torsion scalar is not local Lorentz invariant, the field equations in the TEGR limit is invariant under local Lorentz transformation (LLT). On the contrary, the field equations of the non-linear $f(T)$ are not in general invariant under LLT [Li et al. \(2011\)](#); [Sotiriou et al. \(2011\)](#). This crucial property makes the $f(T)$ teleparallel gravity different from $f(R)$ gravity.

2.4. $f(T)$ cosmology

We assume that the background geometry of the universe is a flat Friedmann-Lemaître-Robertson-Walker (FLRW). Hence, we take the Cartesian coordinate system $(t; x, y, z)$ and the diagonal vierbein

$$e_\mu^a = \text{diag}(1, a(t), a(t), a(t)), \quad (14)$$

where $a(t)$ is the scale factor of the universe. Using (3) and (14), this gives rise to the flat FLRW metric

$$ds^2 = dt^2 - a(t)^2 \delta_{ij} dx^i dx^j, \quad (15)$$

where the Minkowskian signature is $\eta_{ab} = (+, -, -, -)$. We note that this choice of the vierbein (14) leads to consistent field equations without involving any unphysical degrees of freedom for any $f(T)$ theory [Ferraro & Fiorini \(2011\)](#); [Krššák & Saridakis \(2016\)](#). The diagonal vierbein (14) directly relates the teleparallel torsion scalar (4) to Hubble rate as follows,

$$T = -6H(t)^2, \quad (16)$$

where $H(t) \equiv \dot{a}/a$ is Hubble parameter, and the “dot” denotes differentiation with respect to the cosmic time t . Inserting the vierbein (14) into the field equations (12) for the matter fluid (7), the modified Friedmann equations of the $f(T)$ -gravity are,

$$\frac{3}{\kappa^2}H^2 = \rho + \rho_T \equiv \rho_{eff}, \quad (17)$$

$$-\frac{1}{\kappa^2} \left(3H^2 + 2\dot{H} \right) = p + p_T \equiv p_{eff}, \quad (18)$$

where ρ and p are respectively the energy density and pressure of the matter sector, considered to correspond to a perfect fluid. Independently of the above equations, one should choose an equation of state to relate ρ and p . Here, we choose the simple linear barotropic case $p = w\rho$, where w is the equation of state parameter. We are interested in evolution during (pressureless) matter domination, we therefore in practice set $w = 0$. Additionally, the torsional density and pressure in the above equations are

$$\rho_T = \frac{1}{2\kappa^2} [2Tf_T - T - f(T)], \quad (19)$$

$$p_T = \frac{1}{2\kappa^2} \left[\frac{f(T) - Tf_T + 2T^2f_{TT}}{f_T + 2Tf_{TT}} \right], \quad (20)$$

By acquiring the standard matter conservation, we write the continuity equation

$$\dot{\rho} + 3H(\rho + p) = 0. \quad (21)$$

This in return implies the continuity equation of the torsional fluid

$$\dot{\rho}_T + 3H(\rho_T + p_T) = 0, \quad (22)$$

in order to have a conservative universe. We additionally take an equation-of-state parameter $w_T \equiv p_T/\rho_T$ of the torsional fluid, which incorporates the dark energy sector. So we write

$$w_{DE} \equiv w_T = \frac{p_T}{\rho_T} = -1 + \frac{[f(T) - 2Tf_T](f_T + 2Tf_{TT} - 1)}{[f(T) + T - 2Tf_T](f_T + 2Tf_{TT})}. \quad (23)$$

It is useful to define the effective equation-of-state parameter

$$w_{eff} \equiv \frac{p_{eff}}{\rho_{eff}} = -1 - \frac{2}{3} \frac{\dot{H}}{H^2}, \quad (24)$$

which can be related to the deceleration parameter q by the following expression

$$q \equiv -1 - \frac{\dot{H}}{H^2} = \frac{1}{2} (1 + 3w_{eff}). \quad (25)$$

3. TORSIONAL IR CORRECTION MODEL

In this section, we explore the cosmic evolution that arises as a consequence of the $f(T)$ teleparallel gravity

$$f(T) = T + \alpha \frac{T_0^{1+n}}{T^n}, \quad (26)$$

where α and n are dimensionless parameters. We denote the present value of a quantity by a subscript “0”, so T_0 is the present value of the teleparallel torsion scalar (using (16), we have $T_0 = -6H_0^2$). As a matter of fact, the addition $1/T^n$ -term will be effective in the small torsion (i.e Hubble) regime on the large scale, so we would refer to this term as torsional IR correction. As is clear, the model recovers the GR limit at $\alpha = 0$ or in the large T regime, where the orders of magnitudes $O(T^n) \gg O(T_0^{1+n})$. On the other hand, it reduces to Λ CDM at $n = 0$ or in the small T regime, as the magnitudes $O(T^n) \sim O(T_0^{1+n})$, where the quantity $O(\alpha T_0^{1+n}) \approx O(\Lambda)$. Using relation (16), we write the torsional density and pressure (19) and (20) in terms of the Hubble parameter as

$$\rho_T = \frac{3\alpha}{\kappa^2(2n+1)} H_0^2 \left(\frac{H_0}{H} \right)^{2n}, \quad (27)$$

$$p_T = -\frac{3\alpha}{\kappa^2} \frac{(1+3n+2n^2)H_0^{2n+2}H^2}{H^{2n+2} + \alpha(2n+1)H_0^{2n+2}}. \quad (28)$$

Inserting (27) into Friedmann equation (17) at current time, we write

$$\alpha = \frac{1 - \Omega_{m,0}}{2n+1}, \quad (29)$$

where $\Omega_{m,0} = \frac{\rho_0}{3H_0^2/\kappa^2}$ is the current matter density parameter. The above equation shows that only one of the parameters α and n is independent. In addition, we use the constraint $\Omega_{m,0}h^2 = 0.1417$, where $h = H_0/100$, as estimated by the CMB measurements [Planck collaboration XIII \(2016\)](#), in the rest of our calculations. We will discuss this condition in more details later on.

The continuity equation of the CDM gives $\rho(H) = \rho_0/a(H)^3$, where $\rho_0 = 3\Omega_{m,0}H_0^2/\kappa^2$ is the current density. Then, the scale factor reads

$$a^3 = \frac{\Omega_{m,0}H_0^2H^{2n}}{H^{2n+2} - (1 - \Omega_{m,0})H_0^{2n+2}}. \quad (30)$$

Using the scale factor-redshift relation, $z = \frac{a_0}{a} - 1$, where $a_0 = 1$ at present, we write

$$z = \left(\frac{E^2 - (1 - \Omega_{m,0})E^{-2n}}{\Omega_{m,0}} \right)^{\frac{1}{3}} - 1, \quad (31)$$

where $E = H/H_0$. The inverse relation of (31) gives $H(z)$, however for a particular n this could be expressed explicitly but complicated. Later in Section 5, we show the value $n = 1/3$ is preferable by observations. For $n = 1$ case, a simpler form of $H(z)$ is given in appendix A as an example

with other features to show the cosmic history according to the torsional IR correction model. So in the following we focus our discussion on the cases, $n = 0$ which reduces to the Λ CDM scenario, in addition to $n = 1/3$ and $n = 1$ models.

4. COSMIC HISTORY AND THE PHANTOM REGIME

In this section we describe cosmic history in the context of torsional gravity models with IR corrections of the form described in the previous section. We show these corrections can provide a mechanism for an accelerated phase of cosmic expansion. Prior to this the evolution is essentially equivalent to that of the standard model, thermal history and structure formation are therefore not expected to be affected. We evaluate the transition to the accelerated phase and show that this eventually involves a phantom regime. The measurements of the deceleration to acceleration transition and dark energy EoS are not currently precise enough to distinguish our models from the standard one. Current observations that can do are examined in the next section.

4.1. Phase portrait analysis and deceleration-to-acceleration transition

In a recent study [Awad et al. \(2018b\)](#), the dynamical system approach was applied to the ordinary differential equations arising in the context of $f(T)$ cosmologies. This showed that the modified Friedmann equations can be reduced to a *one-dimensional autonomous system*, where $\dot{H} = \mathcal{F}(H)$. It has been proven that the $f(T)$ phase portraits can be analyzed easily and information can be extracted in a clear way (for more applications of this approach to $f(T)$ gravity cosmology see [Bamba et al. \(2016\)](#); [El Hanafy & Nashed \(2017a,b\)](#); [Awad et al. \(2018a\)](#)). In particular, the governing equation is given by

$$\dot{H} = 3(1+w) \frac{f - H f_H}{f_{HH}} = \mathcal{F}(H), \quad (32)$$

where $f = f(H)$, $f_H = \frac{df}{dH}$ and $f_{HH} = \frac{d^2f}{dH^2}$. Inserting the torsional IR correction (26) into the governing equation (32), we can determine the phase portrait equation of the model:

$$\dot{H} = -\frac{3}{2}(1+w)H^2 \left[\frac{(H/H_0)^{2(n+1)} - (1 - \Omega_{m,0})}{(H/H_0)^{2(n+1)} + n(1 - \Omega_{m,0})} \right]. \quad (33)$$

At large Hubble regime, the above equation reduces to

$$\dot{H} \approx -\frac{3}{2}(1+w)H^2,$$

which characterizes the phase portrait in general relativity. The torsional IR correction model thus matches standard predictions of matter domination ($w = 0$), prior to cosmic acceleration, as well as the earlier radiation domination era, $w = 1/3$, era. Indeed, from Eqs. (27) and (28), it is not difficult to show that $\rho_T \rightarrow 0$ and $p_T \rightarrow 0$ as $z \rightarrow \infty$ ($H \rightarrow \infty$). We thus expect that our torsion correction to the teleparallel equivalent to GR will not affect the thermal history and structure formation up to the transition to cosmic acceleration.

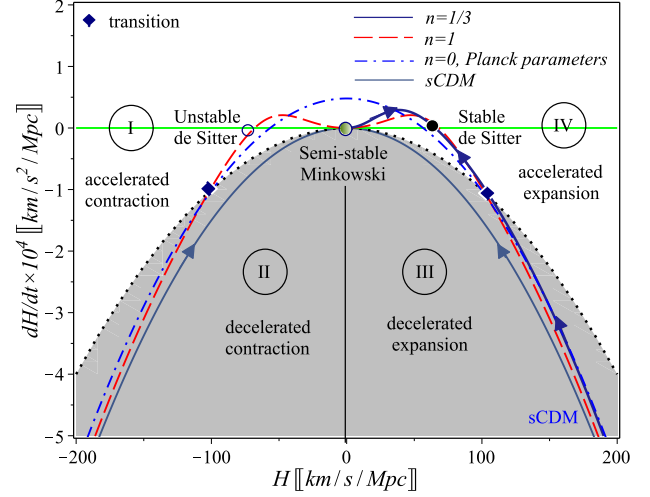


Figure 1. Following the drawing codes in [Awad et al. \(2018b\)](#), the phase portrait (33) of the torsional IR correction matches the s CDM portrait at $H \gg H_{tr}$, while it intersects the zero acceleration curve at H_{tr} and evolving towards a fixed point H_f values. Thus, the model is in agreement with standard cosmology at past and can perform late acceleration in agreement with observations. We use $w = 0$, $\Omega_{m,0} = 0.262$ and $H_0 = 73.5$ km/s/Mpc for $n = 1/3$ and $n = 1$ models, while in $n = 0$ model we use Planck parameters.

In Fig. 1, we visualize the phase portrait (32) for different values of n versus the Λ CDM ($n = 0$) using Planck parameters. As clear the portrait is unbounded from below, where $\dot{H} \rightarrow -\infty$ as $H \rightarrow \infty$, which indicates an initial singularity (Big-Bang), asymptotically the portrait matches the s CDM one in the shaded region III (decelerated expansion). However, it cuts the zero acceleration curve, $q = 0$ (i.e. $\dot{H} = -H^2$), which determines the value of the Hubble parameter at transition H_{tr} . Using (32), we find

$$H_{tr} = [(2n+3)(1 - \Omega_{m,0})]^{\frac{1}{2(n+1)}} H_0. \quad (34)$$

Using the values $H_0 = 73.5$ km/s/Mpc and $\Omega_{m,0} = 0.262$, we obtain $H_{tr} = 107$ (102) km/s/Mpc for $n = 1/3$ ($n = 1$), respectively. For $n = 0$ with Planck parameters (Λ CDM), we find $H_{tr} = 98$ km/s/Mpc. Plugging these results in (31), we determine the transitional redshift $z_{tr} \sim 0.797$ (~ 0.798) for $n = 1/3$ ($n = 1$), respectively. However, for Λ CDM with Planck parameters, it is $z_{tr} \sim 0.649$.

For comparison, we can also pin the predicted transition to cosmic acceleration directly from the evolution of the deceleration parameter. Plugging (33) into (25), we write the deceleration parameter

$$q(z) = -1 + \frac{3}{2} \frac{E(z)^{2n+2} - (1 - \Omega_{m,0})}{E(z)^{2n+2} + n(1 - \Omega_{m,0})}. \quad (35)$$

In Fig. 2, we plot the evolution of the deceleration parameter for different values of n versus the Λ CDM using Planck parameters. The plots show that the deceleration parameter

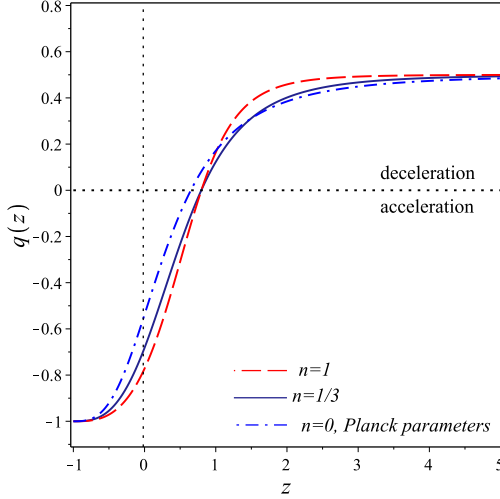


Figure 2. The evolution of the deceleration parameter (35): The plots show that the transition from deceleration to acceleration is at $z_{tr} \sim 0.8$ when $n = 1/3$ and $n = 1$ which is in agreement with observations. For the torsional IR correction model with $n = 1/3$ and 1, we take $\Omega_{m,0}=0.26$ and $H_0=73.5$ km/s/Mpc. For $n = 0$ model (Λ CDM), we use the Planck parameters $\Omega_{m,0} = 0.308$ and $H_0 = 68$ km/s/Mpc.

$q \rightarrow 0.5$ ($w_{eff} \rightarrow 0$) at high redshift which is agreement with the Λ CDM domination. In addition, the transition from deceleration to acceleration occurred at redshift $z_{tr} \approx 0.8$ which is in agreement with the measured value Farooq et al. (2017). Also, the current value of the deceleration parameter $q_0 \approx -0.68$ ($w_{eff} \approx -0.79$).

The portrait crosses the zero acceleration curve to the unshaded region IV (accelerated expansion) and evolves towards a fixed point H_f at $\dot{H} = 0$. This determines the Hubble value at the fixed point

$$H_f = (1 - \Omega_{m,0})^{\frac{1}{2(n+1)}} H_0. \quad (36)$$

Notably, this fixed point cannot be reached in finite time, i.e. $H \rightarrow H_f = \text{constant}$ as $t \rightarrow \infty$, this indicates a pseudo-rip fate Frampton et al. (2012). In the following we show that this is associated with a phantom regime.

4.2. Phantom-like effective DE

In order to investigate the physics of the torsional IR correction, we define its equation of state (23). Substituting from (27) and (28), we obtain

$$w_T(z) \equiv \frac{p_T}{\rho_T} = -1 - n \left[\frac{E(z)^{2n+2} - (1 - \Omega_{m,0})}{E(z)^{2n+2} + n(1 - \Omega_{m,0})} \right]. \quad (37)$$

The inverse relation of Eq. (31) allows to express the torsional EoS in terms of redshift, $w_T(z)$, explicitly. In Fig. 3, we plot the torsional EoS for different choices of the parameter n . We thus determine the current value of the tor-

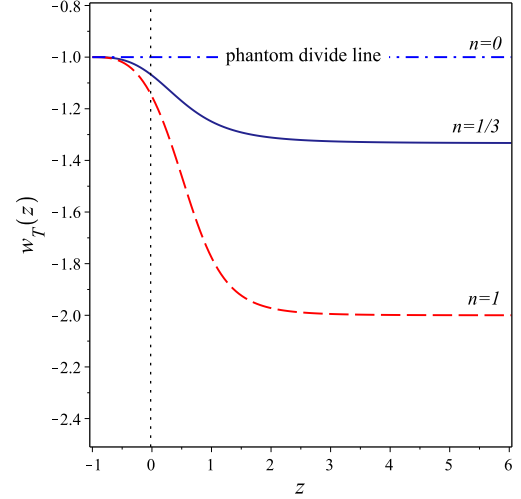


Figure 3. The evolution of the torsional EoS parameter (37): For $n = 1/3$ and $n = 1$, the plots show that the torsional IR correction incorporates a dynamical phantom-like dark energy. At high redshift $w_T \rightarrow -1\frac{1}{3}$ (or -2) where $n = 1/3$ (or $n = 1$), respectively. In both models the torsional fluid evolves towards a cosmological constant $w_T \rightarrow -1$ at far future, therefore the big-rip fate is avoidable in those models. The current value is $w_T = -1.07$ (or -1.15) where $n = 1/3$ (or $n = 1$) in agreement with observational constraints. For $n = 0$, the torsional fluid gives a fixed EoS $w_T = -1$, i.e. cosmological constant.

sional equation of state, $w_T(z = 0) = -1.07$ (-1.15) where $n = 1/3$ ($n = 1$), respectively, which is in agreement with observations Sahni et al. (2014); Di Valentino et al. (2016b, 2017b). We find that the torsional fluid at past fixed to $w_T \rightarrow -1\frac{1}{3}$ (-2) where $n = 1/3$ ($n = 1$) as the redshift $z \rightarrow \infty$, while it is evolving towards the cosmological constant with $w_T \rightarrow -1$ at far future as $z \rightarrow -1$. This confirms that the torsional IR correction incorporates phantom-like dark energy.

As mentioned in the introduction, dynamical phantom-like dark energy is in fact favored by recent observations. Modified gravity can provide for a framework for such scenarios without introducing ghost instabilities associated with scalar field models of phantom dark energy.

Finally, it is worth noting that the invoked phantom regime does not violate age constraints (e.g., such as those derived from old globular clusters) even while using the locally measure value of H_0 . For the proposed model (26), the age of the universe is

$$\begin{aligned} t_{age} &= - \int_{H_0}^{\infty} \dot{H}^{-1} dH \\ &= \frac{2}{3H_0} \int_1^{\infty} E^{-2} \frac{E^{2(n+1)} + n(1 - \Omega_{m,0})}{E^{2(n+1)} - (1 - \Omega_{m,0})} dE. \end{aligned} \quad (38)$$

Even for a large Hubble constant, e.g. $H_0 = 73.5$ km/s/Mpc as measured by local observations Riess et al. (2018) (here-

inafter referred to as R18) and $\Omega_{m,0} \sim 0.262$ (so as to keep $\Omega_{m,0}h^2 = 0.1417$ constant as we discuss below), the model predicts an age $t_{age} \sim 13.6$ (13.9) billion years for $n = 1/3$ ($n = 1$). In conclusion, the model predicts an age of the universe compatible with current observations.

5. CONFRONTATION WITH OBSERVATIONS

In this section, we fix the free parameters of the torsional IR gravity model, n and α (alternatively $\Omega_{m,0}$). We use Planck measurement of the CMB shift parameter at recombination to constrain the value of n according to the H_0 value. In addition, we use the Planck constraint fixing $\Omega_{m,0}h^2 \sim 0.1417$ so that we do not have any deviation from the CMB Planck results. Also, we confront the model predictions of the electron-scattering optical depth at reionization with the Planck measurements. Next we use cosmic chronography (CC) and radial and transverse BAO measurements including Lyman- α observations to examine the model.

5.1. Distance to CMB and shift parameter: resolving the H_0 tension

As is now well known there exists significant tension between the locally measured value of the Hubble constant and that inferred from the CMB. For example, [Riess et al. \(2018\)](#) recently measured $H_0 = (73.52 \pm 1.62 \text{ km/s/Mpc})$, while [Planck collaboration XIII \(2016\)](#) estimate $H_0 = (67.8 \pm 0.9 \text{ km/s/Mpc})$. While the debate continues as to whether the discrepancy is due to new physics or simply observational systematic, it is straightforward to show that the values can in principle be reconciled by invoking a phantom acceleration regime, as we now outline.

Given a primordial fluctuation spectrum and an FLRW cosmology, the relative height of the CMB peaks is essentially determined by the dimensionless physical dark matter and baryon densities $\Omega_c h^2$ and $\Omega_b h^2$, respectively. Fixing, in addition, the number of effective relativistic degrees of freedom in turn fixes the era of matter radiation equality and recombination, and with these the intrinsic physical scale of the CMB peaks (e.g., [Hu & Sugiyama \(1995\)](#); [Percival et al. \(2002\)](#)), as well as light element production in the context of big bang nucleosynthesis (BBN). We will assume that all these parameters are fixed to standard values (namely, as quoted in [Planck collaboration XIII \(2016\)](#)), and that the cosmological evolution is practically indistinguishable from the standard scenario up to late times, when the dark energy like component becomes significant. For the specific case of the modified gravity models used here, the latter assumption is justified by the fact that the IR correction theory tends to the teleparallel equivalent to GR at such redshifts, we thus expect the evolution, including the growth of perturbations, to be similar.

In this context, a measurement of the angular diameter (transverse) distance to the CMB

$$D_A(z) = \frac{1}{1+z} \int_0^z \frac{dz'}{H(z')}, \quad (39)$$

with $z = z_{lss}$ referring to the redshift of last scattering surface, determines H_0 , given a cosmological model (i.e. $H(z)$). In the standard Λ CDM model, such a measurement should yield a value that is smaller than locally measured values (similar to the one obtained by [Planck collaboration XIII \(2016\)](#) by fitting the full CMB spectrum). Nevertheless, as $H(z)$ can be written as $H(z) = H_0 E(z)$, it is easy to see that one can increase H_0 , while keeping the angular distance constant, by choosing a model where $E(z)$ smaller than that associated with Λ CDM in the redshift range $0 \leq z \leq z_{lss}$. This state of affairs would also be reflected in the invariance of the “shift parameter” of [Efstathiou & Bond \(1999\)](#)

$$\mathcal{R}_{lss} = \sqrt{\Omega_{m,0} H_0^2} \int_0^{z_{lss}} \frac{dz}{H(z)} = \sqrt{\Omega_{m,0}} \int_0^{z_{lss}} \frac{dz}{E(z)}. \quad (40)$$

Clearly, if one keeps $\Omega_{m,0}h^2$ constant while increasing H_0 , then $\Omega_{m,0}$ becomes smaller. It is then sufficient for $E(z)$ to be always below its Λ CDM value $E_\Lambda(z)$ for $0 \leq z \leq z_{lss}$, for it to be possible to keep \mathcal{R}_{lss} constant. We now show that this is not only possible but necessary, in the phantom regime, that $E_p(z) \leq E_\Lambda(z)$.

Friedmann evolution in a flat universe with matter and DE (or DE-like, as in torsion gravity) components implies

$$\frac{E_p^2(z)}{E_\Lambda^2(z)} = \frac{\Omega_{mp} a^{-3} + \Omega_p(z)}{\Omega_{m\Lambda} a^{-3} + \Omega_\Lambda} \quad (41)$$

where Ω_{mp} and $\Omega_{m\Lambda}$ refer to the contributions of the matter densities to the critical density at $z = 0$ in the phantom and Λ CDM cases respectively. If one requires a larger value for H_0 in the phantom case, while keeping $\Omega_{m,0}h^2$ the same in the two cases, then $\Omega_{mp} < \Omega_{m\Lambda}$. The contribution Ω_Λ to the current critical density is constant, while $\Omega_p = \Omega_p(z)$, being a phantom DE contribution, necessarily increases in time (with decreasing z).

By definition $E_p(z=0)/E_\Lambda(z=0) = 1$. But since $\Omega_p(z=0) > \Omega_p(z > 0)$, and Ω_Λ is constant, it follows that $\frac{E_p(z)}{E_\Lambda(z)} < 1$ for $z > 0$, even if $\Omega_{mp} = \Omega_{m\Lambda}$. If we require that $\Omega_{mp} < \Omega_{m\Lambda}$, so as to keep $\Omega_{m,0}h^2$ the same while increasing H_0 , then the ratio $\frac{E_p(z)}{E_\Lambda(z)}$ becomes smaller still. It is thus apparent that in the presence of phantom like dark energy, it is not only possible but necessary to decrease $E(z)$ relative to the standard case, which in turn necessitates an increase in H_0 if CMB angular distance, shift parameter and physical matter densities are to be kept constant.

[Fig. 4](#) illustrates this in the context of our torsion gravity models. Here we vary H_0 , keeping $\Omega_{m,0}h^2 = 0.1417$ (as measured in [Planck collaboration XIII \(2016\)](#)), and evaluate the shift parameter \mathcal{R}_{lss} , substituting $H(z)$, namely the inverse of (31), into (40) where $z_{lss} = 1089.9$ [Planck collaboration XIII \(2016\)](#). We then subtract this from the measured value of $\mathcal{R}_{lss} = 1.7488$, retrieved from (Planck TT+lowP) [Planck collaboration XIV \(2016\)](#), and divide by the error estimate quoted therein (± 0.0074). As can be seen, as one deviates from the cosmological constant scenario

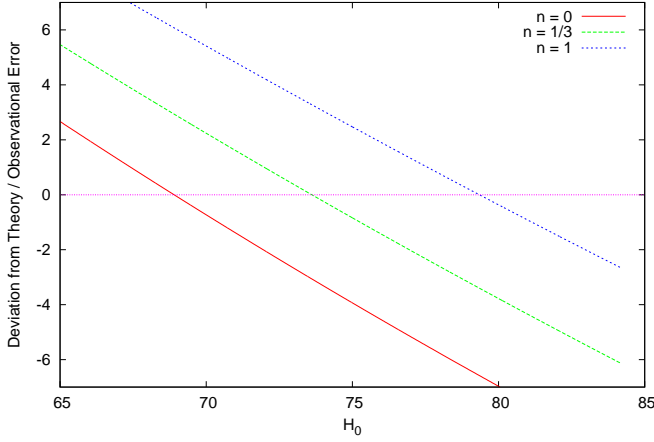


Figure 4. Fixing H_0 via CMB shift parameter. The horizontal line of zero error signifies a perfect fit. An index $n = 0$ corresponds to a cosmological constant, $n = 1/3$ and $n = 1$ refer to departures from this (given by Eq. (26)).

($n = 0$) and further into the phantom regime, the lines intersect the zero error horizontal at larger values of H_0 ; as, expected, these larger values are thus necessary in order to fit the CMB data embodied in the shift parameter. In particular a value of about $n = 1/3$ fits the shift parameter with $H_0 = 73.5$ km/s/Mpc, as locally measured by Riess et al. (2018).

5.2. Reionization redshift

The electron-scattering optical depth τ_e of the CMB, provides a direct probe of the reionization epoch and its redshift z_{re} ; it places constraints on the cosmological model, as it depends on $H(z)$ at redshifts intermediate between z_{lss} and local measurements. The optical depth can be evaluated from

$$\tau_e(z_{re}) = c \int_0^{z_{re}} \frac{n_e(z) \sigma_T dz}{(1+z)H(z)}, \quad (42)$$

where $n_e(z)$ is the electron density and σ_T is the Thomson cross-section describing scattering between electrons and CMB photons. Here we take the densities of hydrogen, helium and electrons, respectively, as $n_H = [(1 - Y_p)\Omega_b \rho_{cr,0}/m_H](1+z)^3$, $n_{He} = y n_H$ and $n_e = (1+y)n_H$, where $y = \frac{Y_p}{4(1-Y_p)}$ and m_H is the hydrogen mass Shull & Venkatesan (2008). We use the Planck constraint $\Omega_{b,0} h^2 = 0.02230$ Planck collaboration XIII (2016), which gives the baryon density parameter $\Omega_{b,0} = 0.0413$ for $H_0 = 73.5$ km/s/Mpc, the helium mass fraction $Y_p = 0.247$ Peimbert et al. (2007) and the current critical density $\rho_{c,0} = 1.88 \times 10^{-29} h^2$ g/cm³. Then, using the inverse function of Eq. (31) and by evaluating the integral (42), we get $\tau_e(z_{re}) \approx 0.058$ at $z_{re} = 8.1$, which is in agreement with Planck collaboration XLVII (2016) (lollipop +

PlanckTT + lensing) observations¹, $\tau_e(z_{re}) = 0.058 \pm 0.012$ where $7.8 < z_{re} < 8.8$.

5.3. Local Hubble parameter evolution

As the resolution of the H_0 tension in terms of phantom dark energy described above involves changing the evolution of $H(z)$ — through changing $E(z)$ — it is natural to inquire whether this change can be actually distinguished directly from local $H(z)$ measurements. Fig. 5 collects such measurements. These include the 43 Hubble measurements given in Cao et al. (2018), which lists a number of CC and BAO measurements (including two Ly- α observations). In addition to the following four BAO measurements: $H(z = 0.978) = 113.72 \pm 14.63$, $H(z = 1.23) = 131.44 \pm 12.42$, $H(z = 1.526) = 148.11 \pm 12.75$ and $H(z = 1.944) = 172.63 \pm 14.79$ km/s/Mpc (Zhao et al. (2018)), and one BAO Ly- α observation $H(z = 2.33) = 224 \pm 8$ km/s/Mpc (du Mas des Bourboux et al. (2017)). This, in addition to the R18 observation of $H_0 = 73.52 \pm 1.62$ km/s/Mpc as measured by Riess et al. (2018). Fig. 5 shows clearly the capability of the torsional IR gravity (with $n = 1/3$) to fit with R18 and Ly- α better than Λ CDM model.

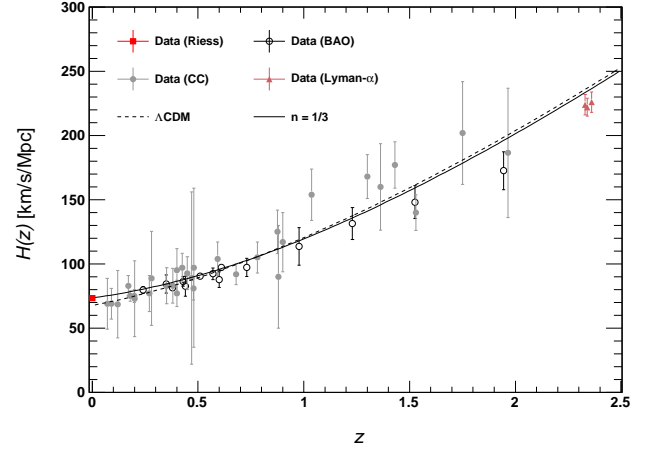


Figure 5. Evolution of Hubble function in terms of redshift: For the Λ CDM model with $n = 0$, we take $H_0 = 68$ km/s/Mpc. For the torsional IR gravity model with $n = 1/3$, we take $H_0 = 73.5$ km/s/Mpc.

¹ We note that torsional IR gravity model is in excellent agreement with the latest Planck results Planck collaboration VI (2018). Using $\Omega_{b,0} h^2 = 0.02242$ which gives the baryon density parameter $\Omega_{b,0} = 0.0415$ for $H_0 = 73.5$ km/s/Mpc, $Y_p = 0.2454$ as predicted by BBN, we get $\tau_e(z_{re}) \approx 0.0553$ at $z_{re} = 7.82$, which is in agreement with Planck collaboration VI (2018) observations (TT,TE,EE+lowE+lensing+BAO), $\tau_e(z_{re}) = 0.0561 \pm 0.0071$ where $z_{re} = 7.82 \pm 0.71$.

The χ^2 statistics of these forty nine Hubble measurements are

$$\chi^2(n, \alpha) = \sum_i \frac{(H_i^t - H_i^o)^2}{\sigma_{H_i^o}^2}, \quad (43)$$

where the subscript $i = 1, 2, \dots, 49$, the superscripts t and o denote respectively the theoretical and the observed values of $H(z_i)$, and $\sigma_{H_i^o}$ denote the one standard deviations in the measured values. As can be inferred from Table 1, both Λ CDM and the model with $n = 1/3$ and $H_0 = 73.5$ km/s/Mpc, display $\chi^2/\text{dof} \lesssim 1$. But the model associated with phantom-like effective dark energy component performs better than that invoking cosmological constant. This remains the case as long the Ly- α and R18 data are included. The BAO data on its own, on the other hand, favors the standard model. As we see below, this conclusion is definitely consolidated by BAO distance measurements, combined with the CMB.

Table 1. the χ^2 calculations of $H(z)$: For $n = 0$ (Λ CDM), we take $H_0 = 68$ km/s/Mpc. For $n = 1/3$ (torsional IR gravity), we take $H_0 = 73.5$ km/s/Mpc.

Dataset	n	χ^2 / dof	χ_{dof}^2
CC	0	14.77 / 29	≈ 0.51
	1/3	16.78 / 29	≈ 0.58
BAO	0	9.59 / 12	≈ 0.80
	1/3	11.39 / 12	≈ 0.95
CC+BAO+R18	0	35.97 / 17	≈ 0.82
	1/3	28.17 / 17	≈ 0.64
CC+BAO+R18+Ly- α	0	44.98 / 47	≈ 0.96
	1/3	33.67 / 47	≈ 0.72

Note: For R18, we take $H_0 = 73.52 \pm 1.62$ km/s/Mpc as measured by Milky Way 50 Gaia + HST, Long P Parallaxes at redshift Riess et al. (2018).

We note that the Hubble function is related to the luminosity-distance $D_L(z)$ by

$$H(z) = \left[\frac{d}{dz} \left(\frac{D_L(z)}{1+z} \right) \right]^{-1}. \quad (44)$$

In fact being Hubble a first derivative of D_L makes it – observationally wise – not a quite well measurable quantity. However, distances are in principle integrable quantities, which makes them relatively more precise. In the following we confront the torsional IR gravity with the BAO angular distance measurements.

5.4. BAO distance measurements

BAO can be used as standard rulers; from isotropic measurements one can infer $D_V = [cz(1+z)^2 D_A^2(z)/H(z)]^{1/3}$

and from anisotropic measurements D_A itself (given the sound horizon at the baryon drag epoch r_d). These measurements rely on the same principle as that used to infer the angular diameter distance to the CMB (as once the physical densities and eras of recombination and matter radiation equality are determined, the physical scale of the peaks is fixed). It turns out that such measurements are highly constraining and essentially rule out solutions of the H_0 tension invoking phantom-like dark energy.

We show this by using the observations from various independent data sets: Beutler et al. (2011) which use 6dFGS data, Kazin et al. (2014) for reconstructed WiggleZ, Ross et al. (2015) for the SDSS MGS data, Alam et al. (2017) for BOSS, , Ata et al. (2018) for eBOSS quasar data. and Abbott et al. (2017) for the DES survey. We use $r_d = 147.5$ Mpc, when the results are given as ratios involving r_d . We calculate the relevant distances to the observed redshift of the BAO peaks of each observation for our torsion models, deriving D_A and D_V for values of $0 \leq n \leq 1$. For each such value, we vary Ω_m to search for the minimum of

$$\chi^2(n, H_0) = \sum_i \frac{(D_i^t - D_i^o)^2}{\sigma_i^2} + \frac{(\mathcal{R}_{lss}^t - \mathcal{R}_{lss}^o)^2}{\sigma_{lss}^2}, \quad (45)$$

where D_i refers to the different BAO measurements (either D_V or D_A , depending on the particular set of observation), σ the one standard deviations in measurements, and the superscripts t and o refer to the theoretical and observed values of the different quantities. For each n there is then a unique Ω_m that minimizes the χ^2 . Assuming, as we do, that $\Omega_{m,0} h^2$ is held fixed (at 0.1417), one can also associate a unique H_0 with each Ω_m , and hence for each Ω_m that minimizes χ^2 at each n .

The results are shown in Fig 6. As can be seen, the deviation between the observed and inferred distances, as measured using (45) is smallest for $n = 0$. Values of $n \gtrsim 1/5$ are ruled out at the 99% confidence level. Moreover for $n = 1/3$, the corresponding H_0 that minimizes χ^2 is significantly smaller than that inferred when fitting the CMB alone in Section 5.1 above. The reason for this failure is discussed in the next section.

5.5. BAO distance measurements and the failure of phantom models

In Section 5.1, we argued that the angular diameter distance to the CMB and the shift parameter can be kept constant if one increases the value of H_0 while invoking cosmic evolution in the phantom regime. This was because $E(z) = H(z)/H_0$ is smaller up to $z = 0$ for such scenarios than in the case when the DE contribution comes from a cosmological constant. Requiring a larger value of H_0 evidently implies that the $H(z)$ associated with phantom dark energy becomes larger than that of Λ CDM at some redshift $z_c \geq 0$. From the Friedmann equations

$$\frac{H_p^2(z)}{H_\Lambda^2(z)} = \frac{\rho_{mp}(z) + \rho_p(z)}{\rho_{m\Lambda}(z) + \rho_\Lambda}, \quad (46)$$

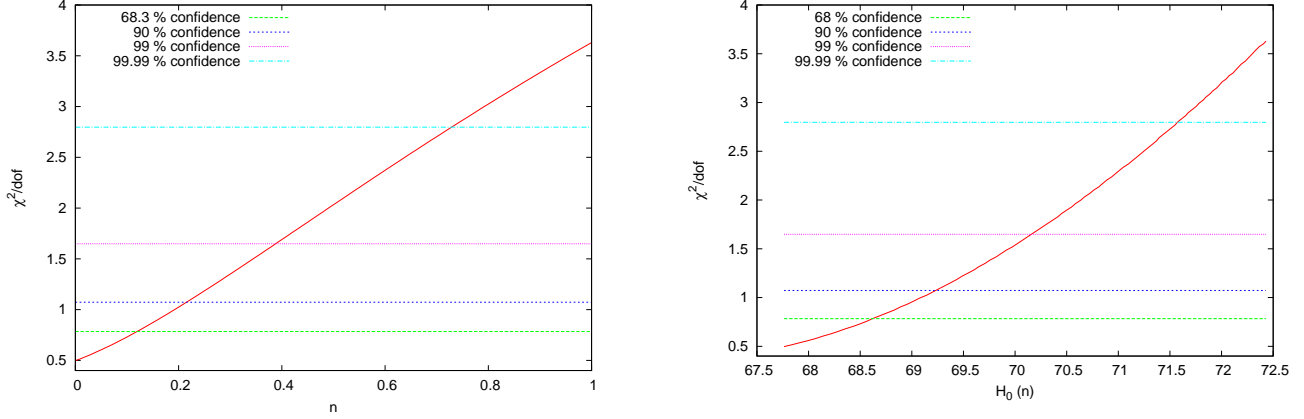


Figure 6. Combined χ^2 per degree of freedom of CMB and BAO distances., with horizontal lines showing the associated confidence levels. Left panel: as a function of n (measuring deviation from cosmological constant at $n = 0$). Right panel: in terms of the value of H_0 that minimizes χ^2 for each value of n (assuming $\Omega_{m,0}h^2 = 0.1417$).

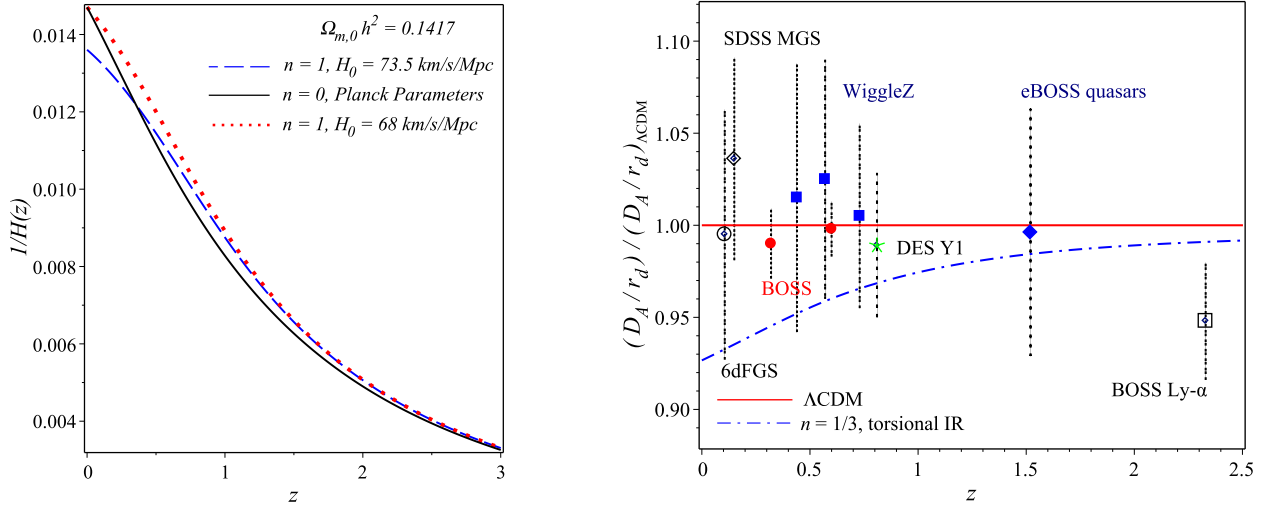


Figure 7. The evolution of the radial and angular distances. Left panel: The redshift evolution of the integrand in Eq. (39). Note that for $n \neq 0$ — i.e., deviation from a cosmological constant and into the phantom regime — $1/H(z)$ is invariably larger if H_0 is kept fixed. This implies larger distances for all z . For larger H_0 the curves of $n = 0$ and $n = 1$ cross. This means that radial distances can be underestimated or overestimated, depending on their location relative to the crossing point. However if the distance to the CMB is fixed, in both models, then the $n > 0$ distances are again invariably smaller. Right panel: Comparison of Λ CDM (horizontal line) and phantom model with $n = 1/3$ and $H_0 = 73.5$ km/s/Mpc with BAO transverse distance estimates. As can be seen phantom models systematically underestimate the transverse distance compared to the Λ CDM, while no such systematics in the data at redshift $z \lesssim 1.5$.

one can find this redshift. The physical matter densities remain such that $\rho_{mp} = \rho_{m\Lambda}$ if we keep $\Omega_{m,0}h^2$ fixed, so that the ratio in (46) is smaller than one when the phantom dark energy density is less than that associated with a cosmological constant: $\rho_p(z) < \rho_\Lambda$. The ration then increases to finally reach $H_p^2(z=0)/H_\Lambda^2(z=0)$ at $z = 0$, which is greater than unity if we assume a larger value of the Hubble constant to be associated with the phantom case. The crit-

ical value z_c corresponds to a ratio one. If this occurs during matter domination, then the epoch where $\frac{H_p^2(z)}{H_\Lambda^2(z)} < 1$ has negligible effect on the evolution and $H_p^2(z) > H_\Lambda^2(z)$ for all practical purposes (that is during DE domination). In this case, the angular diameter distance to the CMB will increase. If the this distance (and shift parameter) are to be kept in line

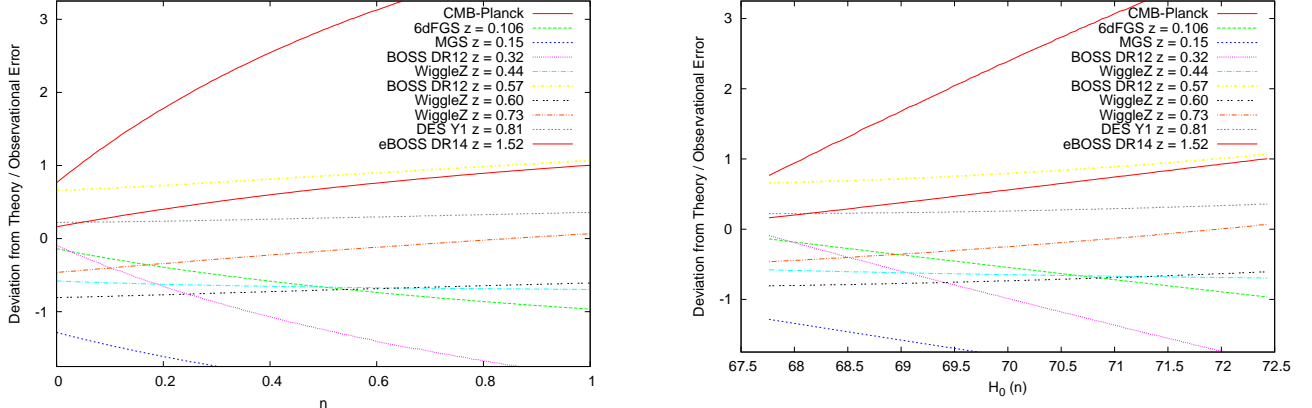


Figure 8. Same as in Fig. 6, but for the individual components of the error vector, showing the error evolution in each observable, with change in n , and associated H_0 .

with observed values then $H_p^2(z) > H_\Lambda^2(z)$ should become unity at $z_c \sim 1$.

In the case of torsion gravity models studied here this is illustrated in Fig. 7, where we plot $1/H(z)$ — the integrand in the formula for the angular diameter distance — for the standard model with $n = 0$ and for $n = 1$. If H_0 assume to be the same in the two case $H(n = 0)$ is always smaller or equal to $H(z = 1)$, which simply reflects the fact that $E_p \leq E_\Lambda$ up to $z = 0$ as expected from the discussion in... When H_0 associated with the $n = 1$ case is larger the lines cross at $z = z_c$. What this implies is that the angular diameter distance will be smaller than in the standard case for objects at $z < z_c$. And if the distance to the CMB $D_A(z = z_{lss})$ is to be kept fixed, while increasing H_0 and invoking the phantom regime, then $D_A(z)$ to any object at $0 \leq z \leq z_{lss}$ will be larger equal to that predicted by Λ CDM. If the distance to the CMB is overestimated, then the distances to objects can be either overestimated or underestimated depending on its redshift.

This implies that, in order to fit CMB and BAO distances simultaneously using a larger H_0 and $n > 0$, the standard model should systematically overestimate distances to BAO measurements, with the discrepancy being maximal for redshifts around z_c . This is not observed, as can be seen from Fig. 7 (right hand panel). To further illustrate the point, we plot the errors associated with the different observations, which were used to estimate the χ^2 in Fig. 8. As can be seen, at $n = 0$ some distances are overestimated and some underestimated, with no clear trend in terms of redshift dependence. As n is varied, the critical redshift z_c changes, and the χ^2 minimization procedure causes the distance to the CMB to also shift. As a result there is another critical redshift below which BAO measurements are underestimate d relative to standard case, and beyond which they are overestimated. Since there is no systematic deviation with respect to Λ CDM predictions in the BAO data used, this process means that some distances that were initially underestimated

at $n = 0$ become even more so for $n > 0$, and conversely some overestimates are increased.

Current CMB and BAO measurements seem to therefore rule out significant phantom-like regime in the redshift range of the BAO data included here. This is the case even if one keep H_0 at a small value; for this would shift the distance to the CMB and also the BOA points due to the smaller $E(z)$ and hence larger associated $1/H(z)$ (as discussed in Section 5.1 and reflected in Fig. 7). We note nevertheless that there seems to be a systematic underestimate of the BAO distances inferred from Lyman- α measurements in the context of Λ CDM. We have not included these points here, as they lead to worse Λ CDM fits and do not lead to much improvement for the cases with $n \neq 0$, given that the models studied here are close to Λ CDM for the relevant redshifts ($z \gtrsim 2$) and the relatively the large observational errors. Possible modest phantom evolution confined to redshifts $z \gtrsim 2$ are therefore not ruled out and can be tested by upcoming data.

6. CONCLUSION

The results presented here suggest that the torsional IR corrections to teleparallel gravity lead to a phantom-like effective dark energy term in the Friedmann equations. Given the current matter density our family of models contain only one free parameter. A phantom-like dark energy evolution, sourced by the gravitational sector can be derived for positive values of this parameter without invoking a canonical scalar field that suffers from ghost instabilities. We perform a dynamical system analysis that elucidates the basic qualitative evolution of the system, including the transition to the accelerated regime.

As has recently been noted, the phantom regime provides a basis for resolving the tension between local and global measurements of the Hubble constant H_0 . We find that these can indeed be reconciled by our model. For values of the parameter that completely reconcile the two values, the phantom regime comes with a dynamical equation of state $-1\frac{1}{3} \leq w_T(z) \leq -1$ with $w_T = -1.07$ at present. These

corresponding deceleration parameter $q_0 = -0.68$ and effective equation of state $w_{eff,0} = -0.79$ at present, with transition redshift $z_{tr} \approx 0.8$. The model also predicts an electron scattering optical depth $\tau_e \approx 0.058$ at reionization redshift $z_{re} \sim 8.1$, which is in agreement with observations.

The model however faces serious problems when baryon acoustic oscillation data are included. This is true for both line of sight measurements, from which the Hubble parameter can be inferred and transverse ones yielding measures of the distances to the BAO peaks at different redshifts. The latter case being most severe; with the model parameter n that corresponds to the reconciliation of the local and CMB values of H_0 is ruled out to more 99.99% confidence by these data.

We argue that this failure should be a generic feature of phantom dark energy models, particularly ones that may solve the H_0 tension by predicting currently observable deviations from Λ CDM evolution at $z \lesssim 2$. For, assuming that $\Omega_{m,0}h^2$ is held constant, so as not to modify the heights of the CMB acoustic peaks, one finds that in fact distances to objects in whole redshift range to the CMB last scattering surface are necessarily overestimated, if the angular diameter distance, and associated shift parameter, are to be kept fixed to current observations. Therefore, if the model predicts currently observable deviations from Λ CDM evolution at $z \lesssim 2$, then it necessarily contradicts the BAO measurements at these redshifts, which do not show any such systematic discrepancies with the standard model. If the distance to the CMB is allowed to shift then the distance to some objects (beyond some critical redshift) will be underestimated

and some (at lower redshift) underestimated, again in a systematic way that is not in line with observations. In this case, we mention some scenarios that possibly resolve the conflict with the angular distance measurements: (i) Phantom models with a sudden ripping behavior at low redshift. As seen from Fig. 7 (the right panel), the non-systematics of the data in fact fit well with models similar to Λ CDM at low redshifts $z \lesssim 1.5$, however in order to fit with large H_0 the model needs to suddenly evolve to phantom regime at $z \lesssim 0.07$, such models may evolve to big-rip singularity or at the best scenario towards a pseudo-rip. In the later one should calculate the ripping inertial force. (ii) Oscillating DE models with quintom behavior (i.e. oscillating about Λ CDM), where phantom behavior should show up at low redshifts $0 < z \lesssim 0.1$ and $z \lesssim 1.5$, quintessence behavior at an intermediate region $0.1 \lesssim z \lesssim 1.5$, and matches Λ CDM at larger redshifts. (iii) Non-flat models, where the contribution of the curvature density parameter Ω_k to the angular distance could provide a correction for better matching with the measured values.

We note that Lyman- α BAO observations at $z \gtrsim 2$ do indeed currently suggest a systematic underestimate on the part of the standard Λ CDM of the distances involved. If these persist with incoming measurements, they could in principle be explained by a phantom regime confined to a range around that redshift.

We would like to thank Adi Nusser and Joe Silk for helpful communication. This work was supported by grant number 25859 from the Egyptian Science and Technology Development Fund Basic and Applied Research Grants.

APPENDIX

A. EXAMPLE: $n = 1$ CASE

As mentioned earlier that Eq. (31) can be inverted to give an explicit Hubble-redshift relation for a particular choice of n . However, this form is complicated to be given in detail. For $n = 1$ model, the formulae are not complicated and can be given explicitly. Since qualitative features are similar to those are discussed for smaller n values, we present $n = 1$ model in detail. In addition, we examine the torsional IR gravity on the perturbation level of the theory by investigating the sound speed c_s of the scalar fluctuations.

A.1. Cosmological parameters

For $n = 1$ case, the torsion gravity model (26) reads

$$f(T) = T + \alpha \frac{T_0^2}{T}. \quad (\text{A1})$$

The modified Friedmanns' equations, (17) and (18), become

$$\rho = \frac{3}{\kappa^2} \left[H^2 - 3\alpha H_0^2 \left(\frac{H_0}{H} \right)^2 \right], \quad (\text{A2})$$

$$p = -\frac{2}{\kappa^2} \dot{H} \left[1 + 3\alpha \left(\frac{H_0}{H} \right)^4 \right] - \rho. \quad (\text{A3})$$

By constraining the above to the linear EoS choice $p = w\rho$, the solution is given as

$$t = t_0 + \frac{2}{3(1+w)H} + \frac{3^{\frac{3}{4}}}{9} \left[\ln \left(\frac{H + (3\alpha)^{\frac{1}{4}} H_0}{H - (3\alpha)^{\frac{1}{4}} H_0} \right) - 2 \arctan \left(\frac{H}{(3\alpha)^{\frac{1}{4}} H_0} \right) \right] \quad (\text{A4})$$

where t_0 is an integration constant. Although, the above solution is exact, it is hard to extract information about the system from (A4). For example, it is not clear how the system could behave at $t \rightarrow \infty$, or how sensitive it is to the choice of initial conditions. On the contrary, as we have shown, the graphical analysis of its phase portrait represents an adequate description of the qualitative features of the global dynamics. For $n = 1$ model, the phase portrait (33) reads

$$\dot{H} = -\frac{3}{2}(1+w)H^2 \left[\frac{(H/H_0)^4 - 3\alpha}{(H/H_0)^4 + 3\alpha} \right], \quad (\text{A5})$$

which has been drawn in Fig. 1. As clear from (A2) and (A3) that the torsional counterpart has density and pressure,

$$\rho_T = \frac{9\alpha H_0^4}{\kappa^2 H^2}, \quad (\text{A6})$$

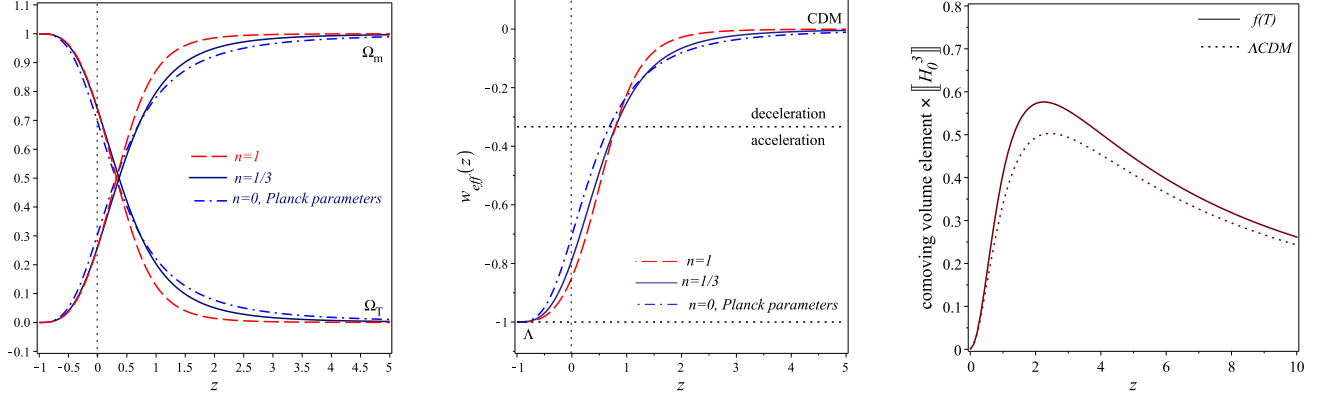


Figure 9. The cosmological parameters of the torsional IR correction. Left panel: The evolution of the matter and the torsional density parameters, $\Omega_m(z)$ and $\Omega_T(z)$, from (A13) and (A14), respectively. Middle panel: The evolution of w_{eff} , namely (A16), shows that the universe effectively matches the CDM with $w_{eff} \rightarrow 0$ at past and evolves towards de Sitter $w_{eff} \rightarrow -1$ as $z \rightarrow -1$ with a transition redshift $z_{tr} = 0.71$ as $w_{eff} = -1/3$. Right panel: The evolution of the volume element (A19) to a factor of H_0^3 .

$$p_T = -\frac{18\alpha H_0^4 H^2}{\kappa^2 (H^4 + 3\alpha H_0^4)}. \quad (A7)$$

It is useful to represent the Friedmann equation (A2) in dimensionless form:

$$\Omega_m + \Omega_T = 1, \quad (A8)$$

where $\Omega_m = \rho/\rho_{eff}$ and $\Omega_T = \rho_T/\rho_{eff}$ are the matter and the torsion density parameters, respectively. Also, we note that the model parameter α , namely Eq. (29), is related to current matter density parameter,

$$\alpha = \frac{1}{3}(1 - \Omega_{m,0}) = \frac{1}{3}\Omega_{T,0}. \quad (A9)$$

Using the above equation and the useful relation

$$\dot{H} = -(1+z)H(z)\frac{dH}{dz}, \quad (A10)$$

one can solve (33) for Hubble

$$H(z) = \frac{H_0}{\sqrt{2}} \sqrt{\Omega_{m,0}(1+z)^3 + \sqrt{\Omega_{m,0}^2(1+z)^6 + 4\Omega_{T,0}}}. \quad (A11)$$

One of the important results which can be directly extracted from (A11) is the age-redshift relation.

$$t(z) = \frac{\sqrt{2}}{H_0} \int_z^\infty \frac{dz'/(1+z')}{\sqrt{\Omega_{m,0}(1+z')^3 + \sqrt{\Omega_{m,0}^2(1+z')^6 + 4\Omega_{T,0}}}. \quad (A12)$$

Next we evaluate the matter density parameter by substituting from (A11) into (A2), which yields

$$\Omega_m(z) = \frac{2\Omega_{m,0}(1+z)^3}{\Omega_{m,0}(1+z)^3 + \sqrt{\Omega_{m,0}^2(1+z)^6 + 4\Omega_{T,0}}}. \quad (A13)$$

Thus, the torsional density parameter is

$$\Omega_T(z) = 1 - \frac{2\Omega_{m,0}(1+z)^3}{\Omega_{m,0}(1+z)^3 + \sqrt{\Omega_{m,0}^2(1+z)^6 + 4\Omega_{T,0}}}. \quad (A14)$$

We plot the evolution of $\Omega_m(z)$ and $\Omega_T(z)$ in Fig. 9(left panel). It shows that $\Omega_m \rightarrow 1$ at large z while $\Omega_T \rightarrow 0$, which indicates the CDM domination. On the contrary, Ω_m drops to zero and $\Omega_T \rightarrow 1$ at $z \rightarrow -1$ ($t \rightarrow \infty$), where the evolution is dominated with the dark torsion with a pseudo-rip cosmology as a final fate. The pattern shown in Fig. 9(left panel) is in agreement with basic requirements of the viable scenario.

Using Eqs. (A10) and (A11), the deceleration parameter of the torsional IR model is given by

$$q(z) = -1 + \frac{3\Omega_{m,0}(1+z)^3}{2\sqrt{\Omega_{m,0}^2(1+z)^6 + 4\Omega_{T,0}}}. \quad (A15)$$

Alternatively, using (25), we write the effective (total) EoS

$$w_{eff}(z) = -1 + \frac{\Omega_{m,0}(1+z)^3}{\sqrt{\Omega_{m,0}^2(1+z)^6 + 4\Omega_{T,0}}}, \quad (A16)$$

which is plotted as in Fig. 9(middle panel), it shows that $-1 \geq w_{eff} \geq -1/3$ at $-1 \geq z \gtrsim 0.7$ in agreement with observations. However, to express the torsional counterpart EoS in terms of redshift, $w_T(z)$, we substitute (A11) into (27) and (28), to write its density and pressure

$$\begin{aligned} \rho_T(z) &= \frac{6\Omega_{T,0}H_0^2}{\kappa^2 [\Omega_{m,0}(1+z)^3 + \sqrt{\Omega_{m,0}^2(1+z)^6 + 4\Omega_{T,0}}]}, \\ p_T(z) &= -\frac{6\Omega_{T,0}H_0^2}{\kappa^2 \sqrt{\Omega_{m,0}^2(1+z)^6 + 4\Omega_{T,0}}}. \end{aligned} \quad (A17)$$

Hence, we obtain the torsional EoS

$$w_T(z) = -1 - \frac{\Omega_{m,0}(1+z)^3}{\sqrt{\Omega_{m,0}^2(1+z)^6 + 4\Omega_{T,0}}}. \quad (\text{A18})$$

At present, $z = 0$, the above equation reduces to

$$w_{T,0} = -1 - \frac{\Omega_{m,0}}{2 - \Omega_{m,0}}.$$

For any value $\Omega_{m,0} > 0$, the torsional EoS goes below -1 . This clarifies the phantom-like nature of the torsional IR corrections. Also, we note that the angular distance, namely (39), allows to perform an important qualitative test, that is the evolution of the comoving volume element within solid angle $d\Omega$ and redshift dz ,

$$dV = \frac{(1+z)^2 D_A^2}{H(z)} d\Omega dz. \quad (\text{A19})$$

This quantity provides a useful test for computing the source counts Newman & Davis (2000). Using (A11) and (39), the evolution of the volume element (up to a factor of Hubble volume H_0^3) is plotted in Fig. 9(right panel). The plot shows that the comoving volume element reaches a maximum value at $z \gtrsim 2$ very similar to the Λ CDM pattern.

A.2. Physical Viability

In addition, we perform a basic test on the perturbation level of the theory which should be carried out for any modified gravity theory, that is the propagation of the sound speed of the scalar fluctuations. As a matter of fact a considerable array of modified gravity theories can describe the late transition of the cosmic acceleration fulfilling the basic requirements on the background level. However, any such theory remains at risk until its description on the perturbation level too fulfills some physical conditions. A necessary condition is for the sound speed of scalar fluctuations to be constrained between $0 \leq c_s^2 \leq 1$. This is required in order to have a stable and causal theory.

To calculate the sound speed we take the longitudinal gauge with two scalars metric fluctuation, that is

$$ds^2 = (1 + 2\Phi)dt^2 - a^2(1 - 2\Psi)dx^2. \quad (\text{A20})$$

This leads to a fluctuation in the teleparallel torsion scalar Cai et al. (2011)

$$\delta T = 12H(\dot{\Phi} + H\Psi).$$

Just as in GR theory, the weak field limit about Minkowski space clarifies that the scalar metric fluctuation Φ plays the role of the gravitational potential. We follow the perturbation equations Cai et al. (2011) up to the linear order, assuming the matter sector is a canonical scalar field ϕ with a lagrangian

$$\mathcal{L}_m = \mathcal{L}_\phi = \frac{1}{2}\partial_\mu\phi\partial^\mu\phi - V(\phi). \quad (\text{A21})$$

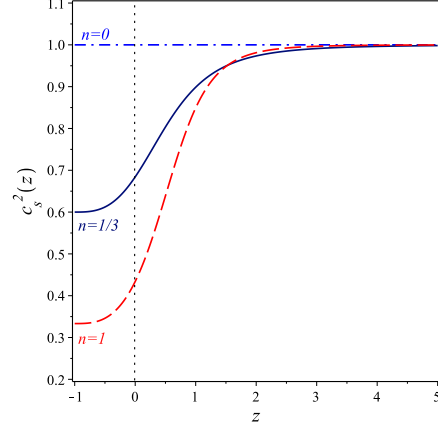


Figure 10. The evolution of the square of the sound speed of the scalar fluctuations (A23). The plots show that $c_s^2(z) \rightarrow 1$ as $z \rightarrow \infty$, for all n values, just as in Λ CDM model, so we do not expect any deviation on the perturbation level of the theory from the standard cosmology. However, for $n = 1$ ($n = 1/3$) models, they evolve towards $c_s^2(z) \rightarrow \frac{1}{3}$ (0.6) as $z \rightarrow -1$ at far future, respectively. This may have some impacts on the modern galaxy formation. In general, the theory is in agreement with the stability and causality conditions as $0 \leq c_s^2 \leq 1$. We use $\Omega_{m,0} = 0.262$ and $H_0 = 73.5$ km/s/Mpc.

For the choice of the vierbein (14), it has been shown that (see Chen et al. (2011); Cai et al. (2011)), in the $f(T)$ gravity, we have only a single degree of freedom minimally coupled to a canonical scalar field ϕ , since the scalar field fluctuation $\delta\phi$ can fully determine the gravitational potential Φ in the absence of anisotropic stress, i.e $\Phi = \Psi$. Using the relation (16), we find that the square of the sound speed² for the general form of the IR $f(T)$ theory (26),

$$c_s^2 = \frac{f_H}{H f_{HH}} = 1 - \frac{2n(1+n)(1 - \Omega_{m,0})}{(1+2n)[\tilde{H}^{2(n+1)} + n(1 - \Omega_{m,0})]}. \quad (\text{A22})$$

As clear, for $n = 0$, the model reduces to Λ CDM where the speed of sound is fixed to the value $c_s = 1$. For $n = 1$ case, we substitute from (A11) into (A22), we write the square of the sound speed in terms of the redshift,

$$c_s^2(z) = 1 - \frac{8\Omega_{T,0}/\sqrt{\Omega_{m,0}^2(1+z)^6 + 4\Omega_{T,0}}}{3\left(\Omega_{m,0}(1+z)^3 + \sqrt{\Omega_{m,0}^2(1+z)^6 + 4\Omega_{T,0}}\right)}. \quad (\text{A23})$$

We thus can verify that the square of the sound speed of the primordial scalar fluctuation $c_s^2 \rightarrow 1$ at past as $z \rightarrow \infty$, while its current value $c_s^2(z = 0) \sim 0.43$. However, at the far fu-

² Usually the square of the sound speed of the scalar fluctuations is given in the form $c_s^2 = \frac{f_T}{f_T + 2T f_{TT}}$ (see Chen et al. (2011); Cai et al. (2011)). We reexpress it in terms of H as given in Eq. (A22), which is more appropriate for our analysis.

ture $c_s^2 \rightarrow \frac{1}{3}$ as $z \rightarrow -1$. The detailed evolution is given in Fig. 10, which shows that the square of the sound speed is $\frac{1}{3} \leq c_s^2 \leq 1$. Also, we include the evolution of $c_s^2(z)$ in the

($n = 1/3$) case for completeness. This result confirms that the torsional IR correction theory is free from ghost instability and acausality problems at all times.

REFERENCES

- Abbott, T. M. C., et al. 2017, Submitted to: Mon. Not. Roy. Astron. Soc. <https://arxiv.org/abs/1712.06209>
- Alam, S., et al. 2017, Mon. Not. Roy. Astron. Soc., 470, 2617, doi: [10.1093/mnras/stx721](https://doi.org/10.1093/mnras/stx721)
- Aldrovandi, R., & Pereira, J. G. 2013, Teleparallel Gravity, Vol. 173 (Dordrecht: Springer), doi: [10.1007/978-94-007-5143-9](https://doi.org/10.1007/978-94-007-5143-9)
- Anderson, L., et al. 2014, MNRAS, 441, 24, doi: [10.1093/mnras/stu523](https://doi.org/10.1093/mnras/stu523)
- Ata, M., et al. 2018, Mon. Not. Roy. Astron. Soc., 473, 4773, doi: [10.1093/mnras/stx2630](https://doi.org/10.1093/mnras/stx2630)
- Awad, A., El Hanafy, W., Nashed, G. G. L., Odintsov, S. D., & Oikonomou, V. K. 2018a, JCAP, 1807, 026, doi: [10.1088/1475-7516/2018/07/026](https://doi.org/10.1088/1475-7516/2018/07/026)
- Awad, A., El Hanafy, W., Nashed, G. G. L., & Saridakis, E. N. 2018b, JCAP, 1802, 052, doi: [10.1088/1475-7516/2018/02/052](https://doi.org/10.1088/1475-7516/2018/02/052)
- Bamba, K., Geng, C.-Q., & Lee, C.-C. 2010, <https://arxiv.org/abs/1008.4036>
- Bamba, K., Geng, C.-Q., Lee, C.-C., & Luo, L.-W. 2011, JCAP, 1101, 021, doi: [10.1088/1475-7516/2011/01/021](https://doi.org/10.1088/1475-7516/2011/01/021)
- Bamba, K., Nashed, G. G. L., El Hanafy, W., & Ibraheem, S. K. 2016, Phys. Rev. D, 94, 083513, doi: [10.1103/PhysRevD.94.083513](https://doi.org/10.1103/PhysRevD.94.083513)
- Bengochea, G. R., & Ferraro, R. 2009, Phys. Rev. D, 79, 124019, doi: [10.1103/PhysRevD.79.124019](https://doi.org/10.1103/PhysRevD.79.124019)
- Bennett, C., et al. 2013, Astrophys.J.Suppl., 208, 20, doi: [10.1088/0067-0049/208/2/20](https://doi.org/10.1088/0067-0049/208/2/20)
- Beutler, F., Blake, C., Colless, M., et al. 2011, MNRAS, 416, 3017, doi: [10.1111/j.1365-2966.2011.19250.x](https://doi.org/10.1111/j.1365-2966.2011.19250.x)
- Cai, Y.-F., Capozziello, S., De Laurentis, M., & Saridakis, E. N. 2016, Rept. Prog. Phys., 79, 106901, doi: [10.1088/0034-4885/79/10/106901](https://doi.org/10.1088/0034-4885/79/10/106901)
- Cai, Y.-F., Chen, S.-H., Dent, J. B., Dutta, S., & Saridakis, E. N. 2011, Class. Quant. Grav., 28, 215011, doi: [10.1088/0264-9381/28/21/215011](https://doi.org/10.1088/0264-9381/28/21/215011)
- Cao, S.-L., Duan, X.-W., Meng, X.-L., & Zhang, T.-J. 2018, Eur. Phys. J., 313, doi: [10.1140/epjc/s10052-018-5796-y](https://doi.org/10.1140/epjc/s10052-018-5796-y)
- Capozziello, S., & De Laurentis, M. 2011, Phys. Rept., 509, 167, doi: [10.1016/j.physrep.2011.09.003](https://doi.org/10.1016/j.physrep.2011.09.003)
- Carroll, S. M., De Felice, A., & Trodden, M. 2005, Phys. Rev., 023525, doi: [10.1103/PhysRevD.71.023525](https://doi.org/10.1103/PhysRevD.71.023525)
- Carroll, S. M., Hoffman, M., & Trodden, M. 2003, Phys. Rev., 023509, doi: [10.1103/PhysRevD.68.023509](https://doi.org/10.1103/PhysRevD.68.023509)
- Cepa, J. 2004, Astron. Astrophys., 422, 831, doi: [10.1051/0004-6361:20035734](https://doi.org/10.1051/0004-6361:20035734)
- Chen, S.-H., Dent, J. B., Dutta, S., & Saridakis, E. N. 2011, Phys. Rev. D, 83, 023508, doi: [10.1103/PhysRevD.83.023508](https://doi.org/10.1103/PhysRevD.83.023508)
- Clifton, T., Ferreira, P. G., Padilla, A., & Skordis, C. 2012, Phys. Rept., 513, 1, doi: [10.1016/j.physrep.2012.01.001](https://doi.org/10.1016/j.physrep.2012.01.001)
- de Andrade, V. C., & Pereira, J. G. 1998, Gen. Rel. Grav., 30, 263, doi: [10.1023/A:1018848828521](https://doi.org/10.1023/A:1018848828521)
- De Felice, A., & Tsujikawa, S. 2010, Living Rev. Rel., 13, 3, doi: [10.12942/lrr-2010-3](https://doi.org/10.12942/lrr-2010-3)
- Di Valentino, E., Linder, E. V., & Melchiorri, A. 2017a, <https://arxiv.org/abs/1710.02153>
- Di Valentino, E., Melchiorri, A., Linder, E. V., & Silk, J. 2017b, Phys. Rev. D, 96, 023523, doi: [10.1103/PhysRevD.96.023523](https://doi.org/10.1103/PhysRevD.96.023523)
- Di Valentino, E., Melchiorri, A., & Silk, J. 2016a, Phys. Rev., 023513, doi: [10.1103/PhysRevD.93.023513](https://doi.org/10.1103/PhysRevD.93.023513)
- , 2016b, Phys. Lett. B, 761, 242, doi: [10.1016/j.physletb.2016.08.043](https://doi.org/10.1016/j.physletb.2016.08.043)
- du Mas des Bourboux, H., et al. 2017, Astron. Astrophys., 608, doi: [10.1051/0004-6361/201731731](https://doi.org/10.1051/0004-6361/201731731)
- Efstathiou, G., & Bond, J. R. 1999, Mon. Not. Roy. Astron. Soc., 304, 75, doi: [10.1046/j.1365-8711.1999.02274.x](https://doi.org/10.1046/j.1365-8711.1999.02274.x)
- El Hanafy, W., & Nashed, G. G. L. 2017a, Chin. Phys. C, 41, 125103, doi: [10.1088/1674-1137/41/12/125103](https://doi.org/10.1088/1674-1137/41/12/125103)
- , 2017b, Int. J. Mod. Phys. D, 26, 1750154, doi: [10.1142/S0218271817501541](https://doi.org/10.1142/S0218271817501541)
- Farooq, O., Madiyar, F. R., Crandall, S., & Ratra, B. 2017, Astrophys. J., 835, 26, doi: [10.3847/1538-4357/835/1/26](https://doi.org/10.3847/1538-4357/835/1/26)
- Ferraro, R., & Fiorini, F. 2011, Phys. Lett., 75, doi: [10.1016/j.physletb.2011.06.049](https://doi.org/10.1016/j.physletb.2011.06.049)
- Frampton, P. H., Ludwick, K. J., & Scherrer, R. J. 2012, Phys. Rev., 083001, doi: [10.1103/PhysRevD.85.083001](https://doi.org/10.1103/PhysRevD.85.083001)
- Hu, W., & Sugiyama, N. 1995, Astrophys. J., 444, 489, doi: [10.1086/175624](https://doi.org/10.1086/175624)
- Huang, Q.-G., & Wang, K. 2016, Eur. Phys. J., 506, doi: [10.1140/epjc/s10052-016-4352-x](https://doi.org/10.1140/epjc/s10052-016-4352-x)
- Kazin, E. A., et al. 2014, Mon. Not. Roy. Astron. Soc., 441, 3524, doi: [10.1093/mnras/stu778](https://doi.org/10.1093/mnras/stu778)
- Kršák, M., & Saridakis, E. N. 2016, Class. Quant. Grav., 33, 115009, doi: [10.1088/0264-9381/33/11/115009](https://doi.org/10.1088/0264-9381/33/11/115009)
- Li, B., Sotiriou, T. P., & Barrow, J. D. 2011, Phys. Rev., 064035, doi: [10.1103/PhysRevD.83.064035](https://doi.org/10.1103/PhysRevD.83.064035)
- Linder, E. V. 2010, Phys. Rev. D, 81, 127301, doi: [10.1103/PhysRevD.81.127301](https://doi.org/10.1103/PhysRevD.81.127301)
- Ludwick, K. J. 2017, Mod. Phys. Lett., 1730025, doi: [10.1142/S0217732317300257](https://doi.org/10.1142/S0217732317300257)

- Newman, J. A., & Davis, M. 2000, *Astrophys. J.*, 534, L11, doi: [10.1086/312657](https://doi.org/10.1086/312657)
- Peimbert, M., Luridiana, V., & Peimbert, A. 2007, *Astrophys. J.*, 666, 636, doi: [10.1086/520571](https://doi.org/10.1086/520571)
- Percival, W. J., et al. 2002, *Mon. Not. Roy. Astron. Soc.*, 337, 1068, doi: [10.1046/j.1365-8711.2002.06001.x](https://doi.org/10.1046/j.1365-8711.2002.06001.x)
- Perlmutter, S., Aldering, G., Goldhaber, G., et al. 1999, *Astrophys. J.*, 517, 565, doi: [10.1086/307221](https://doi.org/10.1086/307221)
- Planck collaboration I. 2016, *Astron. Astrophys.*, 594, doi: [10.1051/0004-6361/201527101](https://doi.org/10.1051/0004-6361/201527101)
- Planck collaboration VI. 2018. <https://arxiv.org/abs/1807.06209>
- Planck collaboration XIII. 2016, *Astron. Astrophys.*, 594, doi: [10.1051/0004-6361/201525830](https://doi.org/10.1051/0004-6361/201525830)
- Planck collaboration XIV. 2016, *Astron. Astrophys.*, 594, doi: [10.1051/0004-6361/201525814](https://doi.org/10.1051/0004-6361/201525814)
- Planck collaboration XLVII. 2016, *Astron. Astrophys.*, 596, doi: [10.1051/0004-6361/201628890](https://doi.org/10.1051/0004-6361/201628890)
- Riess, A. G., Filippenko, A. V., Challis, P., et al. 1998, *The Astronomical Journal*, 116, 1009, doi: [10.1086/300499](https://doi.org/10.1086/300499)
- Riess, A. G., et al. 2016, *Astrophys. J.*, 826, 56, doi: [10.3847/0004-637X/826/1/56](https://doi.org/10.3847/0004-637X/826/1/56)
- . 2018, *Astrophys. J.*, 861, 126, doi: [10.3847/1538-4357/aac82e](https://doi.org/10.3847/1538-4357/aac82e)
- Riess, A. G., Casertano, S., Yuan, W., et al. 2018, *ApJ*, 855, 136, doi: [10.3847/1538-4357/aaadb7](https://doi.org/10.3847/1538-4357/aaadb7)
- Ross, A. J., Samushia, L., Howlett, C., et al. 2015, *Mon. Not. Roy. Astron. Soc.*, 449, 835, doi: [10.1093/mnras/stv154](https://doi.org/10.1093/mnras/stv154)
- Sahni, V., Shafieloo, A., & Starobinsky, A. A. 2008, *Phys. Rev. D*, 78, 103502, doi: [10.1103/PhysRevD.78.103502](https://doi.org/10.1103/PhysRevD.78.103502)
- . 2014, *The Astrophysical Journal Letters*, 793, doi: [doi:10.1088/2041-8205/793/2/L40](https://doi.org/10.1088/2041-8205/793/2/L40)
- Sahni, V., & Starobinsky, A. 2006, *Int. J. Mod. Phys.*, 2105, doi: [10.1142/S0218271806009704](https://doi.org/10.1142/S0218271806009704)
- Shull, J. M., & Venkatesan, A. 2008, *Astrophys. J.*, 685, 1, doi: [10.1086/590898](https://doi.org/10.1086/590898)
- Sotiriou, T. P., Li, B., & Barrow, J. D. 2011, *Phys. Rev.*, 104030, doi: [10.1103/PhysRevD.83.104030](https://doi.org/10.1103/PhysRevD.83.104030)
- Wang, Y., Xu, L., & Zhao, G.-B. 2017, *Astrophys. J.*, 849, 84, doi: [10.3847/1538-4357/aa8f48](https://doi.org/10.3847/1538-4357/aa8f48)
- Zhao, G.-B., et al. 2017, *Nat. Astron.*, 1, 627, doi: [10.1038/s41550-017-0216-z](https://doi.org/10.1038/s41550-017-0216-z)
- . 2018. <https://arxiv.org/abs/1801.03043>